Back Cover: Integrating 31 P DOSY NMR Spectroscopy and Molecular Mechanics as a Powerful Tool for Unraveling the Chemical Structures of Polyoxomolybdate-Based Amphiphilic Nanohybri...

ARTICLE *in* CHEMISTRY · APRIL 2014

Impact Factor: 5.73 · DOI: 10.1002/chem.201304969 · Source: PubMed

6 AUTHORS, INCLUDING:

Pavletta Shestakova
Bulgarian Academy of Sciences
18 PUBLICATIONS **63** CITATIONS
SEE PROFILE

Gregory Absillis
University of Leuven
32 PUBLICATIONS **406** CITATIONS
SEE PROFILE

Francisco Martin-Martinez
Massachusetts Institute of Technology
18 PUBLICATIONS **129** CITATIONS
SEE PROFILE

Tatjana N Parac-Vogt
University of Leuven
144 PUBLICATIONS **2,867** CITATIONS
SEE PROFILE

ChemPubSoc Europe

DOI: 10.1002/chem.201304969

CHEMISTRY
A European Journal
Full Paper

Organic–Inorganic Hybrids

Integrating ^{31}P DOSY NMR Spectroscopy and Molecular Mechanics as a Powerful Tool for Unraveling the Chemical Structures of Polyoxomolybdate-Based Amphiphilic Nanohybrids in Aqueous Solution

Pavletta Shestakova,[a, b] Gregory Absillis,[b] Francisco J. Martin-Martinez,[c] Frank De Proft,[c] Rudolph Willem,[d] and Tatjana N. Parac-Vogt*[b]

Abstract: Novel organic–inorganic hybrids of various sizes were generated by reaction of 1,8-octanediphosphonic acid (ODP) and $(NH_4)_6Mo_7O_{24}$ in aqueous solution. The formation of rodlike hybrids with variable numbers of covalently bound ODP and polyoxomolybdate (POM) units can be tuned as a function of increasing $(NH_4)_6Mo_7O_{24}$ concentration at fixed ODP concentration. The chemical structure of the ODP/POM hybrids was characterized by ^{1}H, ^{31}P, and ^{95}Mo NMR spectroscopy. Heteronuclear ^{31}P DOSY (diffusion-ordered NMR spectroscopy) and molecular mechanics (MM) calculations were applied to determine the size and shape of the nanosized hybrids generated at various ODP/POM ratios. For this purpose, the structures of ODP/POM hybrids with variable numbers of ODP and POM units were optimized by MM and then approximated as cylinder-shaped objects by using a recently described mathematical algorithm. The thus-obtained cylinder length and diameter were further used to calculate the expected diffusion coefficients of the ODP/POM hybrids. Comparison of the calculated and experimentally determined diffusion coefficients led to the most probable ODP/POM hybrid length for each sample composition. The ^{31}P DOSY results show that the length of the hybrids increases with increasing POM concentration and reaches a maximum corresponding to an average of 8 ODP/7 POM units per chain at a sample composition of 20 mM ODP and 14 mM POM. With excess POM, above the latter concentration, the formation of shorter-chain hybrids terminated by Mo_7 clusters at one or both ends was evidenced on further increasing the POM concentration. The results demonstrate that the combination of ^{31}P DOSY and MM, although virtually unexplored in POM chemistry, is a powerful innovative strategy for the detailed characterization of nanosized organic–inorganic POM-based hybrids in solution.

Introduction

Polyoxometalates (POMs) are a versatile class of metal–oxygen clusters containing early transition metals in their highest oxidation states.[1,2] They display broad diversity in size, shape, charge, acidity, solubility, electrochemical behavior, photochemical properties, and magnetic characteristics. Therefore, they are widely investigated in various research domains including catalysis,[2,3] medicine,[4–6] and materials science.[7,8] During the last decade it was demonstrated that, by covalently linking a POM with well-defined chemical and physical properties (charge, size, shape, redox properties, and acidity) to an organic moiety, hybrid nanostructures with tailor-made functionality and morphology can be engineered, and thus the applications of POMs are expanded from the molecular to the nanodimension. For example, hydrophobic tails can be covalently grafted onto the surface of a hydrophilic Anderson-type Mn POM[9] to create an amphiphilic POM hybrid that self-assembles into vesicles.[10,11]

Several methods to graft organic tails onto POM surfaces have been developed.[2] Most commonly, 2-amino-2-hydroxymethylpropane-1,3-diol (TRIS) molecules functionalized with an

[a] Assoc. Prof. P. Shestakova
NMR Laboratory, Institute of Organic Chemistry with Centre of Phytochemistry
Bulgarian Academy of Sciences
Acad. G. Bontchev Str., B1.9, Sofia 1113 (Bulgaria)

[b] Assoc. Prof. P. Shestakova, Dr. G. Absillis, Prof. T. N. Parac-Vogt
KU Leuven, Department of Chemistry
Molecular Design and Synthesis, Laboratory of Bioinorganic Chemistry
Celestijnenlaan 200F, 3001 Leuven (Belgium)
Fax: (32) 16-32-79-92
E-mail: Tatjana.Vogt@chem.kuleuven.be

[c] Dr. F. J. Martin-Martinez, Prof. F. De Proft
Department of General Chemistry (ALGC)
Vrije Universiteit Brussel (VUB)
Pleinlaan 2, 1050 Brussels (Belgium)

[d] Prof. R. Willem
Department of Materials and Chemistry (MACH)
Vrije Universiteit Brussel (VUB), Pleinlaan 2
1050 Brussels (Belgium)

Supporting information for this article is available on the WWW under http://dx.doi.org/10.1002/chem.201304969.

aliphatic chain were used as tripodal ligands to attach the aliphatic chain to the POM.[12–17] Another frequently used method is the incorporation of organoalkoxysilanes into the POM framework,[18] but in general conceptually new approaches for creating covalently grafted hybrid POMs are limited. Several studies demonstrated that, in the presence of phosphate, the heptamolybdate $[Mo_7O_{24}]^{6-}$ was converted to the pentamolybdodiphosphate $[P_2Mo_5O_{23}]^{6-}$ under mildly acidic conditions.[19,20] The $[P_2Mo_5O_{23}]^{6-}$ anion consists of a five-membered ring, composed of five edge/corner-sharing MoO_6 octahedra, grafted on each side by a phosphate group (Figure 1).[21] This

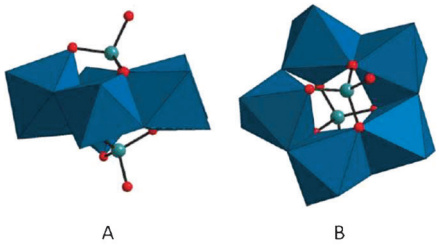

Figure 1. Polyhedral representation of the $[P_2Mo_5O_{23}]^{6-}$ anion consisting of five MoO_6 octahedra and two phosphate groups. A) Side view and B) top view of the five-membered Mo_5 ring with a phosphate group grafted on each side.

phenomenon was also observed in reactions in which the hydrolytic activity of $[Mo_7O_{24}]^{6-}$ towards DNA and RNA model systems was examined by some of us,[22–25] as $[Mo_7O_{24}]^{6-}$ was transformed into $[P_2Mo_5O_{23}]^{6-}$ on release of phosphate as one of the hydrolysis products. Similarly to inorganic phosphate, small aromatic phosphonates can be incorporated into a $(RP)_2Mo_5$-like structure, which demonstrates the ability of P_2Mo_5 units to act as a platform for organic functionalization of POMs.[26–30] The reactivity of $[Mo_7O_{24}]^{6-}$ towards formic acid was also demonstrated.[31]

The majority of POM nanohybrids reported so far were obtained in mixtures of organic solvents and water. In the present work, novel POM nanohybrids based on the P_2Mo_5 system were synthesized by reaction of the difunctional 1,8-octanediphosphonic acid (ODP) with the heptamolybdate $[Mo_7O_{24}]^{6-}$ in pure water as a solvent. In this approach, the POM hybrid is simply generated in situ by mixing the two components, with the benefit that lengthy multistep chemical procedures[9,32] are avoided. We preferred phosphonates over organic phosphates to overcome phosphoester bond hydrolysis in molybdate solutions. In addition, the C–P bond of phosphonates is more stable than the C–O–P moiety of organic phosphates.[22–25] However, monophosphonates are well-known amphiphilic molecules that tend to self-assemble into undesired precipitates that are too versatile and too complex for consistent analysis.[33] On the other hand, diphosphonates such as ODP display a lower tendency to precipitate and offer the additional advantage that they can accommodate two POM clusters per diphosphonate unit, and are thus amenable to obtaining higher POM contents in the generated supramolecular hybrids, which favor their solubility in water. Furthermore, due to the bifunctional nature of ODP, elongated, oligomeric, nanosized hybrids can be formed, which are referred to hereafter as ODP/POM hybrids.

Herein, we demonstrate that well-defined hybrid nanostructures based on ODP and oxomolybdate can be obtained by using this water-based strategy. Varying the molar ODP:$[Mo_7O_{24}]^{6-}$ ratio leads to well-identifiable mixtures of such ODP/POM hybrids. The structure, size, and shape of the these organic/inorganic hybrids were characterized by a combination of ^{31}P diffusion-ordered NMR spectroscopy (DOSY)[34–36] and ^{95}Mo NMR spectroscopy. In the last decade, DOSY NMR has been widely used for the investigation of interactions and aggregation phenomena, including complex colloidal systems[37–42] and supramolecular[43–45] and organometallic complexes.[46–48] However, its use for the characterization of POM-based mixtures is still underexplored, with only few recent papers on ^1H DOSY.[12,17,23,49–53] This gap opens perspectives for new practical developments of DOSY in the challenging and innovative research field of POM-based nanohybrids. Here we demonstrate the potential of heteronuclear ^{31}P DOSY as a powerful and novel strategy for detailed characterization of the size and shape of these new ODP/POM hybrids with the aim of understanding the basis of subsequent formation of aggregates at the micrometric level.[16,17] Molecular mechanics (MM) calculations were performed to determine the geometric parameters of the generated ODP/POM hybrids in order to simulate their translational diffusion characteristics. A comparison of the calculated and experimentally determined diffusion coefficients enabled us to identify the nature of POM/ODP hybrids as a function of sample composition.

Results and Discussion

Multinuclear NMR characterization of the ODP/POM hybrids

In a typical experiment, 20 mM of ODP ($H_2O_3P(CH_2)_8PO_3H_2$) was mixed with 2–100 mM of $(NH_4)_6Mo_7O_{24}$ in reaction mixtures containing 1 mL of D_2O under conditions that favor the formation of P_2Mo_5 systems.[54] The interaction of ODP and $(NH_4)_6Mo_7O_{24}$ was evidenced by characteristic changes in the ^1H, ^{31}P, and ^{95}Mo NMR spectra of the solutions recorded immediately after mixing as a function of sample composition. On adding increasing amounts of $(NH_4)_6Mo_7O_{24}$, the intensity of the ^1H NMR signals for free ODP centered around 1.27 and 1.47 ppm gradually decreased and new ones centered at 3.56, 2.11, 1.96, 1.76, 1.37, and 1.26 ppm appeared (Supporting Information, Figure S1). These results indicate conversion of free ODP to bound ODP. However, due to severe overlap and broad signals in the ^1H NMR spectra, they were not very informative for detailed characterization of the ODP/POM hybrids. However, ^{31}P NMR spectra were much more suitable for this purpose, due to the distinct difference in chemical shift of the signals of free and bound ODP. For example, the ^{31}P NMR spectrum of 20 mM of ODP in the presence of 2 mM of $(NH_4)_6Mo_7O_{24}$ is shown in Figure 2a. The spectrum shows two new signals at 35.95 and 27.98 ppm, in addition to the signal at 27.93 ppm for free ODP. The peak at 35.95 ppm is characteristic for phos-

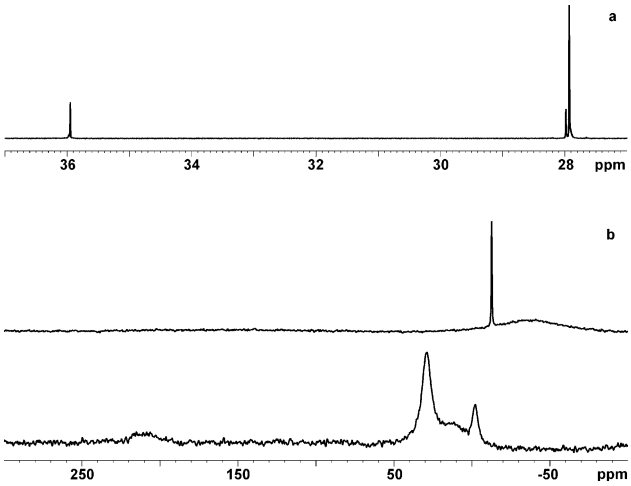

Figure 2. a) ^{31}P spectrum of 20 mM ODP and 2mM POM. b) ^{95}Mo spectra of an aqueous solution of pure $(NH_4)_6Mo_7O_{24}$ (lower trace) and a mixture of 20 mM ODP and 5 mM $(NH_4)_6Mo_7O_{24}$ (upper trace).

phonate-bound P_2Mo_5 clusters.[27] Taking into account the bifunctionality of ODP and its large stoichiometric excess with respect to the POM, it can be assumed that the two new signals originate from in-situ-generated ODP/POM hybrids with two ODP structural units, each of which is covalently bound at one side of a pentamolybdate cluster to form a rodlike structure of the type $\{(H_2PO_3)C_8H_{16}(PO_3)Mo_5O_{15}(PO_3)C_8H_{16}(PO_3H_2)\}^{4-}$ (Figure 3). The signal at 35.95 ppm was assigned to the PO_3

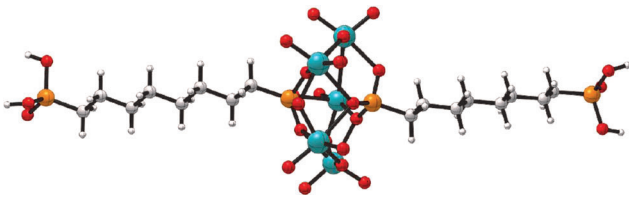

Figure 3. Rodlike hybrid structure with two ODP molecules bound covalently at each side of a single pentamolybdate cluster, as evidenced by ^{31}P NMR spectroscopy on a solution of 20 mM ODP and 2 mM $(NH_4)_6Mo_7O_{24}$.

moiety directly bound to the molybdate cluster, and that at 27.98 ppm to the terminal unbound PO_3 group (Figure 3). Formation of this $[P_2Mo_5O_{23}]^{6-}$-type structure was further evidenced by ^{95}Mo NMR spectroscopy. Figure 2b shows the ^{95}Mo NMR spectrum of the $(NH_4)_6Mo_7O_{24}$ cluster in the absence of ODP with its three characteristic broad resonances at 213, 33, and 14 ppm, as well as a peak around 0 ppm resulting from all other minor Mo species present at the specific pH value used.[55] In the presence of 5 mM $(NH_4)_6Mo_7O_{24}$, the three broad resonances of $(NH_4)_6Mo_7O_{24}$ disappear from the ^{95}Mo NMR spectrum. The new narrow ^{95}Mo signal at −1.42 ppm is characteristic of the P_2Mo_5 cluster, as evidenced previously for $[P_2Mo_5O_{23}]^{6-}$.[24] The ^{95}Mo NMR spectra of P_2Mo_5 clusters typically display such a single narrow peak due to their higher symmetry in comparison to $(NH_4)_6Mo_7O_{24}$. In addition, the broad hump observed upfield from the sharp signal indicates the presence of various unbound Mo species in mutual exchange. Their presence as minor species was also evidenced previously by Lyxell et al. in molybdophenylphosphonate solutions.[54]

The ^{31}P spectra of mixtures at various $(NH_4)_6Mo_7O_{24}$ concentrations (Figure 4) reveal that, on increasing the $(NH_4)_6Mo_7O_{24}$ concentration, the signals of both the unbound PO_3 moiety of

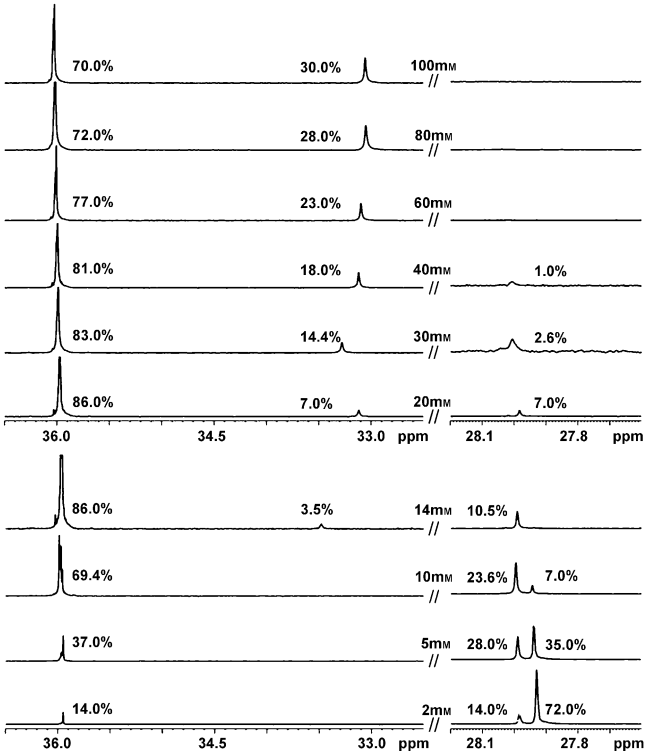

Figure 4. ^{31}P NMR spectra of ODP/POM solutions as a function of $(NH_4)_6Mo_7O_{24}$ concentration at fixed ODP concentration of 20 mM. Relative signal areas are given next to each resonance. The signal at 27.93 ppm corresponds to free ODP, while the signals at 27.98 and 35.95 ppm correspond to the unbound and bound phosphonate moiety of ODP molecules after incorporation into the P_2Mo_5 framework, respectively. The signal at 33.56 ppm corresponds to terminal phosphonate groups bound to Mo_7.

the hybrid species (27.98 ppm) and free ODP (27.93 ppm) decrease in intensity and finally disappear at a high excess of $(NH_4)_6Mo_7O_{24}$. This indicates that increasing the $(NH_4)_6Mo_7O_{24}$ concentration triggers further interactions between the free $H_2O_3P^-$ moieties of these new structures and the added $(NH_4)_6Mo_7O_{24}$ toward formation of longer ODP/POM hybrid chains.

To gain deeper insight into the size, shape, and structure of the ODP/POM hybrids generated at different ODP/POM ratios, a strategy integrating DOSY and ^{95}Mo NMR spectra with MM calculations was used. The precise determination of the diffusion coefficients of the different species present in ODP/POM mixtures from their ^{1}H DOSY spectra is hampered by severe signal overlap in the chemical-shift dimension (Supporting Information, Figure S1). To avoid this problem ^{31}P DOSY NMR was used, as the chemical-shift difference between bound and free ODP is much larger in the ^{31}P chemical-shift dimension (Figure 4).

General approach for the interpretation of diffusion coefficients

DOSY NMR spectroscopy is a powerful method for the investigation of complex mixtures that exploits differences in diffusion coefficients D and particle size as a means of spectroscopic discrimination between the components of the mixture. A DOSY spectrum represents a two-dimensional matrix correlating the chemical shifts of the resonances of the different structural moieties (the horizontal scale) to their diffusion coefficients (the vertical scale). Because the measured diffusion coefficient generally reflects the molecular size and shape, species with different sizes and/or molar masses are differentiated.[34–36]

The translational diffusion coefficient D_t of a particle is related to the particle size and shape through the translational friction coefficient f_t, according to the Stokes–Einstein equation [Eq. (1)],[56] in which T is the temperature and k_B the Boltzman constant.

$$D_t = \frac{k_B T}{f_t} \tag{1}$$

For the simple case of a spherical particle, Equation (2) holds in which η is the solvent viscosity and R_0 the hydrodynamic radius of the particle.

$$f_t = 6\pi\eta R_0 \tag{2}$$

For particles of nonspherical shape, other equations are applied to correlate the translational diffusion coefficient to the geometrical characteristics of the particles and their hydrodynamic properties.[57–59] We chose a strategy in which, starting from theoretical calculations of their molecular geometry, the ODP molecule and the ODP/POM hybrids can be well approximated with cylinder-shaped objects. For a cylinder of finite length the friction coefficient f_t^{cyl} is expressed as Equation (3)[59–62]

$$f_t^{cyl} = f_0 \frac{(2/3)^{1/3} P^{2/3}}{\ln P + \gamma} \tag{3}$$

where $f_0 = 6\pi\eta R_0$ is the friction coefficient of a sphere with radius R_0 and a volume equal to the volume of a cylinder with aspect ratio $P = L/d$, where $L = 2a$ is the cylinder length and $d = 2b$ is its diameter. By using the sphere-to-cylinder volume ratio, R_0 is calculated as Equation (4).

$$R_0 = \frac{1}{2}\sqrt[3]{\frac{3}{2}Ld^2} \tag{4}$$

In Equation (3), γ is the so-called end-effect term, which according to Tirado and de la Torre[59–62] for a randomly oriented rod is given as Equation (5) in which was derived and is strictly valid for aspect ratios $P = 2$–20.

$$\gamma = 0.312 + 0.565/P + 0.100/P^2 \tag{5}$$

By using the above formula for the translational friction coefficient, the translational diffusion coefficient of a cylinder with aspect ratio P and length L is expressed as Equation (6).

$$D_t^{cyl} = \frac{k_B T}{3\pi\eta} \frac{\ln P + \gamma}{L} \tag{6}$$

In the present work, the measured diffusion coefficients D_{exptl} were used to assess the size and shape of the ODP/POM hybrids generated on mixing ODP and $(NH_4)_6Mo_7O_{24}$. To gain insight into the chemical structures of ODP/POM hybrids generated at different mixture compositions and to calculate their diffusion coefficients, we simulated various potential structures with variable numbers of alternating ODP and POM units by means of MM calculations. Particular emphasis was put on the conformational spaces that can be covered by the very flexible hydrocarbon chain of the ODP ligand in order to identify the conformers with lowest energy for a given chain length. The optimized structures of these model rodlike ODP/POM hybrids were used to derive the geometrical parameters a and b, and their diffusion coefficients D_{calcd} were calculated by using Equation (6). The theoretically calculated diffusion coefficients D_{calcd} were then compared to the experimental values D_{exptl} in order to find the ODP/POM hybrids matching best the experimental diffusion coefficients at a given sample composition.

The initial step of the investigation was to measure the diffusion coefficient of the ODP ligand in the absence of POM. The molecular geometrical parameters a and b were determined by MM optimization of the ODP structure and were used in Equation (6) to determine the D_{calcd} value of ODP. The reasonable agreement between $D_{exptl} = 4.84 \times 10^{-10}\ m^2 s^{-1}$, determined from the ^{31}P DOSY spectrum of 20 mM ODP in D_2O (pD 5.18), and $D_{calcd} = 5.50 \times 10^{-10}\ m^2 s^{-1}$, calculated by using the cylinder-shape approximation [Eq. (6)], demonstrated the relevance of our approach.

MM simulations of the ODP/POM hybrids

Universal force field (UFF) MM calculations[63] were performed on various ODP/POM hybrids comprising 1–10 POM clusters, as described in the Experimental Section, with the aim of modeling the rodlike ODP/POM hybrids. This required first calculating the spatial coordinates of all the ODP/POM hybrids as a function of all possible conformations potentially adopted by the very flexible organic ODP ligand bridging two POM cluster units. Although MM is not the most advanced computational method available nowadays, the results provided by UFF match specifically our needs at reduced computational cost, since they provide a general description of the different possible conformational geometries that the ODP/POM hybrids can adopt.

Various geometrical features are needed to describe the hybrids under consideration. Each $[P_2Mo_5O_{21}]^{4-}$ cluster has two P atoms located at opposite sides (Figure 1). These P atoms have a tetrahedral configuration formed by three O atoms and the aliphatic chain (see Figures 3 and 5), which was kept fixed throughout the optimizations. The relative orientation of the

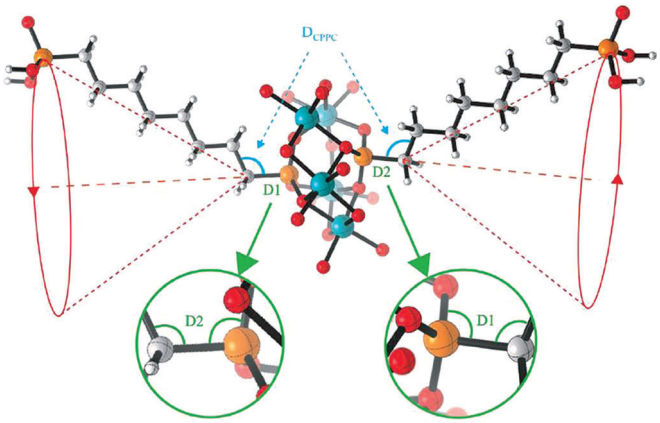

Figure 5. Conformational spaces covered by the aliphatic polymethylene chain of the ODP ligands. Dihedral angles D1 and D2, which characterize the rotation of the polymethylene chains, are shown in green. The tetrahedral coordination configuration of the P atoms is magnified in the green circles. The dihedral D_{CPPC} angle is shown in blue.

aliphatic ODP chain with respect to the cluster was defined by the dihedral angles D1 and D2 between the dicoordinated O atom, the P atom, and the first two C atoms of the ODP chain. These dihedral angles are given as D1 and D2 (shown in green in Figure 5) for each side of the $[P_2Mo_5O_{21}]^{4-}$ cluster. The conformational space covered by D1 and D2 is shown as red cones in Figure 5. These internal rotations of the aliphatic ODP chains determine the dynamic conformational behavior of the ODP/POM hybrids. Finally, the dihedral angle formed by the first C atom of each ODP chain and the P atoms of the cluster (D_{CPPC}, marked in blue in Figure 5) defines the mutual relative orientation of these ODP chains. When this dihedral angle is 180° the ODP chains are oriented in the most extended, linear conformation and the length of the ODP/POM hybrid achieves its highest possible value.

The X-ray coordinates of the $[P_2Mo_5O_{21}]^{4-}$ cluster from the literature[64] were used as initial geometry to start the MM optimizations of the POM in each ODP/POM hybrid. In a preliminary step, we focused on the basic ODP/POM building block of the nanohybrids (Figure 3) comprising a single POM cluster and two pendant ODP units. Taking all possible combinations of D1 and D2 values from 0 to 360° in steps of 45°, each geometry corresponding to such a pair of D1/D2 values was allowed to relax to an optimized geometry at the level of all atoms of both the cluster and the chain dihedral angles. Thus, the full conformation space of D1 and D2 was sampled "digitally" to give an energy space for the ODP/POM hybrid comprising in total $9\times9=81$ fully optimized geometries. In other terms, the full conformational space is screened with a torsional angle resolution of 45°. Of the 81 energy points sampled, 66 converged to energy minima characterized by D1 and D2 values of +61 or −61° each. The uncertainty range in these values never exceeded 4°. From this it was concluded that four potential wells are present in the conformational space. Next, the full potential-energy surface (PES) including not only the potential wells, but also possible energy maxima and/or saddle points, was explored by allowing the atom parameters to fully relax at fixed pairs of D1 and D2 values. Repeating this procedure on varying D1 and D2 in steps of 45° led to the full PES displayed in Figure 6. Analysis of this PES revealed roughly nine different energy ranges of conformational interest, mutually differing by no more than 15 kcal mol^{-1}. Four D1 and D2 ranges—[0–90°; 0–90°], [270–360°; 0–90°], [0–90°; 270–360°], and [270–360°; 270–360°]—correspond to shallow energy wells (blue zones in Figure 6) in which the energy varies from 0 to roughly 5 kcal mol^{-1}. The four other D1 and D2 ranges—[0–90°; 135–225°], [135–225°; 0–90°], [135–225°; 270–360°], [270–360°; 135–225°]—correspond to shallow energy saddle points with barriers of no more than 8 kcal mol^{-1} separating the above-mentioned potential wells. Finally, in the unique pair of D1 and D2 ranges [135–225°; 135–225°], a broad energy peak of 15 kcal mol^{-1} appears in the center of the PES (brown-red zone in Figure 6). An important finding is that the energy barriers separating the four potential wells never exceed 8 kcal mol^{-1} (pale beige regions in the PES of Figure 6). Thus, the ODP chains exhibit essentially unhindered internal rotations, which at room temperature can be considered to be fast on any NMR timescale.

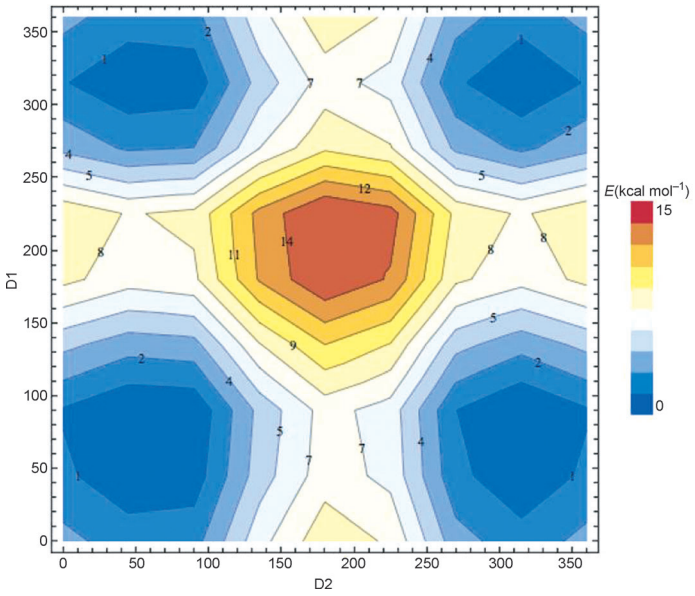

Figure 6. Contour plot of the PES resulting from rotation around the D1 and D2 dihedral angles of the ODP chain for a single $[P_2Mo_5O_{21}]^{4-}$ cluster structure, as defined in Figure 5. For limiting the computation time needed, each of the torsion angles D1 and D2 was varied from 0 to 360° in steps of 45°, and full relaxation of all atoms coordinates was allowed for each pair of D1 and D2 values.

Next, for the sake of calculating the diffusion coefficients for the most representative conformations of ODP/POM nanohybrids for variable numbers of alternating ODP and POM units, we first explored the broadest possible panel of conformations for the ODP/POM hybrid with 11 ODP moieties and 10 POM cluster units, which we believe to be representative for all

ODP/POM nanohybrids ranging from 2 ODP/1 POM to 11 ODP/10 POM. Using the D1 and D2 values of some representative optimized ODP/POM energy minima (e.g., 60, 300°) or saddle points (e.g. 60°, 180°) generated in the previous step, we explored a broad selection of linear rodlike ODP/POM hybrids having up to 10 clusters that can be constructed from the basic ODP/POM unit. We also explored ranges of dihedral angles that lead to ring-shaped nanohybrids. For each ODP/POM rodlike hybrid, each geometry corresponding to such a pair of D1/D2 values was again allowed to relax to an optimized geometry at the level of all clusters and all chain dihedral angles. Figures S2 and S3 (Supporting Information) show the results of such geometry optimizations for a broad selection of conformational arrangements of 10 POM and 11 ODP units in both rodlike and ring-shaped nanohybrids, together with the resulting D1, D2, and D_{CPPC} values defining the relative orientation of the ODP chains at each side of the POM clusters.

When ODP/POM hybrids have very different values of D1 and D2, two dihedral sequences must be considered, namely, D1–D2–D1–D2 and the D1–D2–D2–D1 (e.g., hybrids a and b in Figure S2 of the Supporting Information). The very similar energies of all these ODP/POM hybrids, on the one hand, and the similar conformations of the cluster units in the hybrids and in their isolated form, on the other, strongly suggest that these linear rodlike ODP/POM hybrids are conformationally very dynamic. Indeed, optimization of the hybrids provided very similar D1 and D2 values, typically within a range of 5° each, for all units along the linear hybrid. The rodlike hybrids shown in Figure S2 (Supporting Information) obviously fulfill this finding, but any other rodlike hybrids with different pairs of D1/D2 values within individual ODP/POM units are possible as well and differ only little in energy, and hence basically an infinite number of ODP/POM hybrid conformations with very similar energy is possible. Concerning the geometrical dimensions of interest for the calculation of the diffusion coefficients, we first focused on the rodlike linear hybrids. For this purpose, we used a mathematical algorithm recently described by Petitjean and implemented in software.[65] In short, this software calculates the smallest enclosing cylinder covering a set of points defined by their spatial coordinates in an Euclidean space. In the present context of the rodlike ODP/POM hybrids, these Euclidean points correspond to the spatial coordinates of all the atoms in the ODP/POM hybrids, as obtained by the above MM calculation procedure. Such cylindrical models were shown to be appropriate for the estimation of calculated diffusion coefficients.[61,66,67] The smallest enclosing cylinder calculated for the 11 ODP/10 POM hybrid is given as an example in Figure S4 of the Supporting Information.

The structural data for the hybrid structures (Figure S2) and the calculated diffusion coefficients D_{calcd} (Table S1) can be found in the Supporting Information. The diffusion coefficients of these conformers are very similar, with a difference between the lowest ($0.67\times10^{-10}\,m^2s^{-1}$) and the highest ($0.78\times10^{-10}\,m^2s^{-1}$) D_{calcd} values of no more than $0.11\times10^{-10}\,m^2s^{-1}$, which can hardly be discriminated in the ^{31}P DOSY spectra, given the chemical-shift overlap of their ^{31}P resonances. Considering the very small energy difference between the various conformations of Figure S2 (Supporting Information), we can assume that they are nearly equally populated in the ODP/POM mixture, and the average diffusion coefficient of $0.73\times10^{-10}\,m^2s^{-1}$ can be considered to be representative of the rodlike ODP/POM hybrids with 10 POM cluster units bound together by 11 ODP ligands.

Using this approach we calculated the geometrical parameters for the three lowest-energy conformational arrangements a–c in Figure S2 of the Supporting Information for ODP/POM hybrids of different length varying from 2 ODP/1 POM to 11 ODP/10 POM units. The resulting geometrical parameters $2a$ and $2b$ of these three selected conformations of the optimized model hybrid structures of different hybrid chain lengths and their calculated diffusion coefficients D_{calcd} are listed in Table 1 and were further used for the interpretation of the DOSY data. Table 1 reveals that for the ODP/POM hybrid with structure a, the cylinder length $2a$ increases in increments of about 14 Å for each additional ODP/POM unit. Its diameter $2b$ starts at 9.4 Å for the ODP/POM with two ligands and asymptotically approaches 14.1 Å from six ODP ligands onwards. Structure b shows alternating increments of about 11 and 15 Å, a diameter that again tends to an asymptotic value (here 17.8 Å), and has a higher cylinder thickness but a slightly shorter length. Struc-

Table 1. Structural parameters, optimized by MM calculations, for three different conformational arrangements of the ODP/POM hybrids with variable numbers of alternating ODP and POM units and D_{calcd} values. See Figure S2 (Supporting Information) for the three selected conformations a, b, and c used for the calculations of the diffusion coefficients.

		Structure a			Structure b			Structure c			Averaged conformations
ODP units	Mo_5O_{21} units	$2a$ [Å]	$2b$ [Å]	$10^{10}D_{calcd}$ [m^2s^{-1}]	$2a$ [Å]	$2b$ [Å]	$10^{10}D_{calcd}$ [m^2s^{-1}]	$2a$ [Å]	$2b$ [Å]	$10^{10}D_{calcd}$ [m^2s^{-1}]	$10^{10}D_{calcd,av}$ [m^2s^{-1}]
2	1	28.7	9.4	2.24	28.7	9.4	2.24	28.7	9.4	2.24	2.24
3	2	42.4	11.4	1.68	42.7	10.7	1.71	44.2	8.5	1.86	1.75
4	3	56.3	13.0	1.35	53.8	15.7	1.27	59.3	10.0	1.47	1.36
5	4	70.3	13.8	1.16	68.8	16.6	1.08	74.2	10.0	1.28	1.18
6	5	84.7	14.1	1.03	79.7	17.4	0.98	89.0	9.9	1.15	1.05
7	6	98.8	14.1	0.94	95.5	17.8	0.87	103.8	10.0	1.04	0.95
8	7	112.8	14.1	0.87	107.1	17.8	0.82	118.7	10.0	0.95	0.88
9	8	126.9	14.1	0.81	122.3	17.8	0.75	133.5	10.1	0.87	0.81
10	9	140.9	14.1	0.75	133.9	17.8	0.71	148.3	10.2	0.81	0.76
11	10	154.9	14.1	0.71	148.4	17.8	0.67	162.0	10.3	0.76	0.71

ture c, the cylinder length $2a$ of which increases from 28.7 to 162.0 Å, shows the longest cylinder lengths and smallest diameters in comparison with the other two conformations, which result in the highest D_{calcd} values. The averaged D_{calcd} values, under the reasonable assumption of equal populations of the three selected lowest-energy structures a, b, and c, are listed in Table 1. The non-rod ODP/POM hybrids (Supporting Information, Figure S3) tend to adopt helicoidal conformations. In fact, the highly packed helical shape of the ODP/POM hybrid suggests the possible formation of nanosized rings. Therefore, this possibility was also explored (Supporting Information, Figure S3 q, r, and s). According to our calculations, a ring-shaped hybrid with 11 POM units retains the characteristic D1 and D2 values of the linear ODP/POM hybrids. The latter were also the subject of calculations of diffusion coefficients for comparison with experimental values.

The reason why we considered ODP/POM hybrids with variable numbers of alternating ODP and POM units in our MM and diffusion-coefficients calculations is that our experimental DOSY data clearly displayed variations of the diffusion coefficient of the ligand as a function of the POM concentration. This can only be ascribed, as demonstrated hereafter, to the formation of ODP/POM hybrids of variable chain lengths, that is, with variable number of ODP/POM unit pairs. The D_{exptl} values of the samples prepared with a fixed ODP concentration of 20 mM and POM concentrations ranging from 2 to 100 mM are listed in Table 2 and graphically depicted in Figure 7. The D_{exptl} values decreased from 2.51×10^{-10} to 0.87×10^{-10} m^2s^{-1} on increasing the POM concentration from 2 to 14 mM. Further increasing the POM concentration from 20 to 100 mM resulted in a gradual increase of D_{exptl} from 0.95×10^{-10} to 2.18×10^{-10} m^2s^{-1}. These changes in diffusion coefficients result from structural modifications of the ODP/POM hybrids as a function of sample composition (see below).

Table 2. Diffusion coefficients $10^{10}D_{exptl}$ [m^2s^{-1}] determined from four different signals in the ^{31}P NMR spectra of ODP/POM mixtures as a function of the $(NH_4)_6Mo_7O_{24}$ concentration.

$c(Mo_7)$ [mM]	Peak 3 35.95 ppm	Peak 4 33.56 ppm	Peak 2 27.98 ppm	Peak 1 27.93 ppm
0				4.84
2	2.51		2.57	4.28
5	2.45		2.39	3.87
10	1.33		1.91	3.73
14	0.87	1.26	1.24	
20	0.95	1.32	1.36	
30	1.17	1.61		
40	1.30	1.79		
60	1.71	2.30		
80	1.93	2.36		
100	2.08	2.76		

Analysis of the diffusion coefficients for systems with an excess of ODP by ^{31}P DOSY NMR

Formation of the rodlike structure of type $\{(H_2PO_3)C_8H_{16}(PO_3)Mo_5O_{15}(PO_3)C_8H_{16}(PO_3H_2)\}^{4-}$ (Figure 3) at the lowest

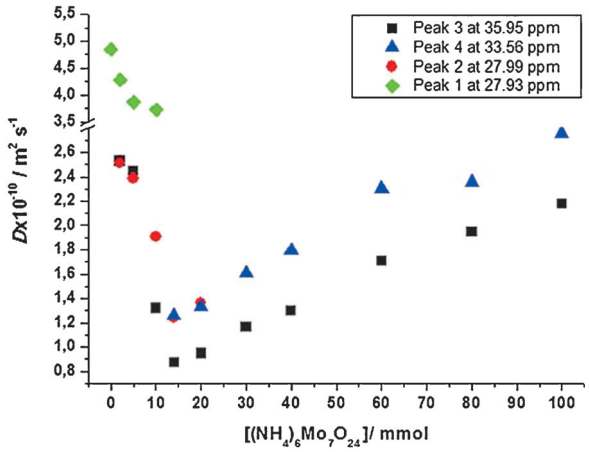

Figure 7. Variation of the diffusion coefficients of the signals observed in the ^{31}P NMR spectra of the ODP/POM mixtures as a function of $(NH_4)_6Mo_7O_{24}$ concentration (mM). The signal at 27.93 ppm corresponds to free ODP, while the signals at 27.99 and 35.95 ppm correspond to the unbound and bound phosphonate moiety of ODP molecules after incorporation into the P_2Mo_5 framework, respectively. The signal at 33.56 ppm corresponds to terminal phosphonate groups bound to Mo_7.

$(NH_4)_6Mo_7O_{24}$ concentration of 2 mM is evidenced by the fact that in the ^{31}P DOSY spectrum the signals corresponding to the PO_3 units bound to the POM cluster ($\delta=35.95$ ppm) and to the unbound PO_3 moieties ($\delta=27.98$ ppm) have identical diffusion coefficients (Figure 8). The diffusion coefficient of 2.24×10^{-10} m^2s^{-1} (Table 1) calculated for the structure shown in Figure 3 by using Equation (6) and the optimized geometrical parameters from MM calculations is in reasonably good agreement with the D_{exptl} value of 2.51×10^{-10} m^2s^{-1} determined for the 20 mM ODP/2 mM $(NH_4)_6Mo_7O_{24}$ mixture. The deviation of about 10% may be due to experimental inaccuracy in the determination of the D_{exptl} value due to the low signal-to-noise ratio of the ^{31}P signal of the hybrid in the presence of

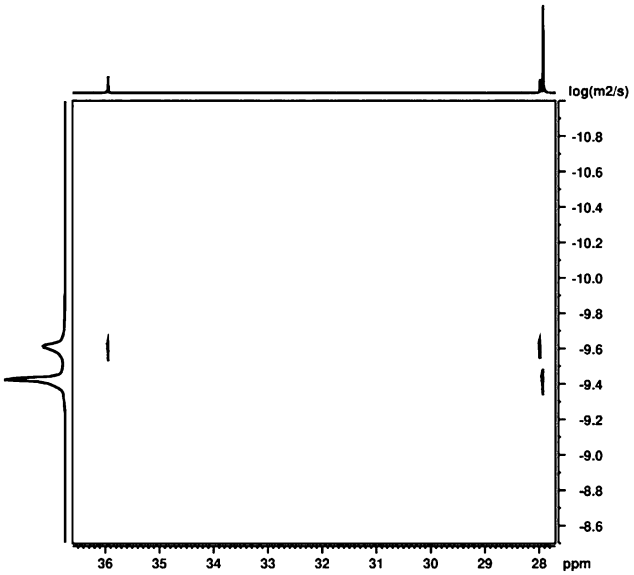

Figure 8. ^{31}P DOSY spectrum of a mixture of 20 mM ODP and 2 mM $(NH_4)_6Mo_7O_{24}$.

the much stronger signal of the free ligand (Figure 4). The spectrum also shows the presence of free ODP molecules ($\delta =$ 27.93 ppm) with larger diffusion coefficient ($D_{exptl} = 4.28 \times 10^{-10}\ m^2\ s^{-1}$), reasonably close to that measured for a pure 20 mM ODP solution ($D_{exptl} = 4.84 \times 10^{-10}\ m^2\ s^{-1}$).

The formation of ODP/POM hybrids with longer chains is supported by the further gradual decrease in the D_{exptl} values of the samples with 5, 10, and 14 mM of $(NH_4)_6Mo_7O_{24}$ (Table 2 and Figure 7). For example the comparison of the experimental and calculated diffusion coefficients (Tables 1 and 2) shows that the D_{exptl} value of $1.33 \times 10^{-10}\ m^2\ s^{-1}$ measured for the sample with 10 mM of $(NH_4)_6Mo_7O_{24}$ matches best an average diffusion coefficient calculated for hybrid structures with four ODP and three POM units when considered on the basis of the D_{exptl} value from the ^{31}P signal at 35.95 ppm. Figure 7 reveals the lowest D_{exptl} values for the system with 14 mM $(NH_4)_6Mo_7O_{24}$. This is precisely the concentration at and above which the ^{31}P signal of free ODP (27.93 ppm) no longer appears (Figure 4), that is, all ODP is bound to POM clusters.

Comparing the lowest experimental diffusion coefficient of $0.87 \times 10^{-10}\ m^2\ s^{-1}$ measured for the resonance of the cluster-bound PO_3 group at 35.95 ppm with the values calculated for the three selected ODP/POM rodlike structures a, b, and c (Table 1 and Figure S2 of the Supporting Information) reveals that the experimental value best reflects the averaged D_{calcd} value of $0.88 \times 10^{-10}\ m^2\ s^{-1}$ calculated for the 8 ODP/7 POM hybrid. However the D_{calcd} values for structure b with 7 ODP/6 POM units and structure c with 9 ODP/8 POM units are also in excellent agreement with the experimental value at this sample composition. Given the high degree of conformational flexibility, which tends to interconvert these conformations for a given chain length, it can be concluded that at 14 mM $(NH_4)_6Mo_7O_{24}$ the maximum length is achieved and is likely distributed from 7/6 to 9/8 ODP/POM pairs.

Figure 7 and Table 2 also reveal that the D_{exptl} values of the signals at 35.95 and 27.98 ppm for the bound and terminal PO_3 groups show increasing discrepancy with increasing $(NH_4)_6Mo_7O_{24}$ concentration. This implies chain-length diversity in the ODP/POM hybrids formed at a given POM concentration, which differ by one or at most two ODP and POM units. If so, given their very similar D values, it is not possible to associate each measured diffusion coefficient with a single chain length of these ODP/POM hybrids. Thus, the measured diffusion coefficients represent population-weighted averages over ODP/POM hybrids of various lengths. The mean value of the diffusion coefficient of the signal at 35.95 ppm is in addition averaged over the different numbers of bound PO_3 groups in the chains of different lengths, which makes this average more sensitive to the presence of longer species. The chemical-shift distribution observed for the signal centered at 35.95 ppm is also indicative of a slight diversity in chemical environments of the ^{31}P atoms along the chain length (Supporting Information, Figure S5). On the other hand, since in each ODP/POM hybrid the number of terminal PO_3 groups is always two, independent of its length, the diffusion coefficient at 27.98 ppm depends on the population of all ODP/POM hybrids and, for a given distribution of chain lengths, is more sensitive to the short hybrids. Moreover the diffusion coefficients of the terminal groups may be also influenced by their rotational motion, which results in a higher apparent diffusion coefficient. This effect is observed for polymeric chains, for which the signals from the terminal chain fragments often show higher D_{exptl} values than the internal ones.[68;69] This explains why D_{exptl} values are always lower for the PO_3 group bound to the POM cluster than for the terminal PO_3 groups. Since the signal at 35.95 ppm has the highest intensity and originates from internal phosphonate moieties, it can be stated that their D_{exptl} value is more representative of the entire hybrid. For clarity and simplicity of further interpretation of results, we base subsequent discussions on the D_{exptl} values determined from this signal only.

In view of these results, the mixture with 14 mM of $(NH_4)_6Mo_7O_{24}$ can be considered to be a threshold composition. Indeed, at this concentration a new signal appears at 33.56 ppm, which indicates that the PO_3 moiety acquires a different structural environment, while the signal of free ODP at 27.93 ppm is no longer observed.

Analysis of the diffusion coefficients for the systems with stoichiometric excess of POM

^{31}P NMR spectroscopy

The intensity of the ^{31}P signal at 33.56 ppm increases on further increasing the POM concentration above the threshold concentration of 14 mM from 20 to 100 mM, while in parallel the intensity of the signal at 27.98 ppm for the terminal unbound PO_3 group of the ODP/POM hybrids decreases and finally vanishes at 60 mM $(NH_4)_6Mo_7O_{24}$ (Figure 4). The disappearance of this signal indicates that at a POM excess above 40 mM, a POM cluster binds to the PO_3 groups on both ends of the ligand. The different chemical shift of the new signal in the ^{31}P spectrum indicates that this PO_3 group and the PO_3 group bound to the Mo_5O_{21} cluster (35.95 ppm) have different chemical environments. According to literature data for mixtures of phenylphosphonic acid (PhP) and polyoxomolybdates at pH 5 with a fivefold excess of POM, an equilibrium exists between the $Mo_5(PhP)_2^{4-}$ and Mo_7PhP^{5-} clusters, hereafter referred to Mo_5 and Mo_7 clusters, for simplicity.[54] Since at pH 5 no Mo_6PhP^{2-} is present, it is therefore proposed that the new signal at 33.56 ppm is assigned to PO_3 groups bound to an Mo_7 cluster, which is also in agreement with the PO_3 chemical-shift data reported by Kobayashi et al. for $[CH_3PMo_7O_{25}(OH)]^{5-}$.[27]

Since ODP is bifunctional, we conclude from the ^{31}P chemical shifts that all samples with $(NH_4)_6Mo_7O_{24}$ concentrations of 14 mM and above are complex mixtures of ODP/POM hybrids with variable numbers of ODP ligands bridging Mo_5 clusters and terminated at one or both ends by Mo_7 units. At least three types of ODP/POM hybrids can be considered to potentially be present in the reaction mixture (Figure 9). The simplest is a rodlike structure with two terminal Mo_7 clusters bound to a single ODP ligand, designated as Hybrid Ia (Figure 9A). To the best of our knowledge, no crystallographic data are available for Mo_7PhP^{5-}-type clusters, so they are rep-

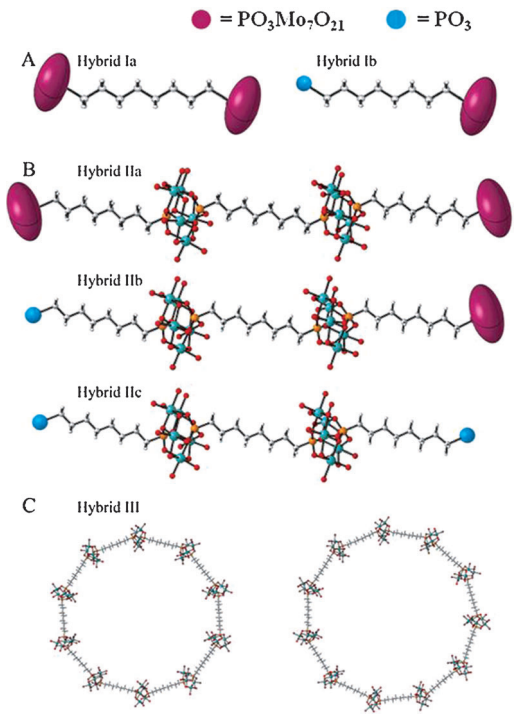

Figure 9. Different types of ODP/POM hybrids potentially generated in ODP/POM samples with $(NH_4)_6Mo_7O_{24}$ in excess.

resented by red ellipsoids. For this symmetric ODP/POM hybrid, only one ^{31}P signal around 33.5 ppm is expected. For $(NH_4)_6Mo_7O_{24}$ concentrations from 14 to 40 mM, an ODP/POM hybrid in which a single ODP ligand is bound to an Mo_7 cluster (Hybrid Ib, Figure 9A) should also be considered, since the signal at 27.93 ppm still reveals the presence of unbound PO_3 moieties. Another possible longer hybrid with rodlike structure is Hybrid II (Figure 9B), in which a variable number of ODP/POM building blocks are linked together along a chain terminated on one or both sides by a PO_3 group bound to an Mo_7 cluster. These hybrids can be described by the general formula $\{(Mo_7O_{21})_k[(PO_3)C_8H_{16}(PO_3)Mo_5O_{15}]_n(PO_3)C_8H_{16}(PO_3)(Mo_7O_{21})_m\}^{x-}$ ($k=0$, 1; $m=0$, 1). In the example of Figure 9B, n equals 2. Because of the different chemical environments of the Mo_5 and Mo_7 clusters, the terminal and internal PO_3 groups have different ^{31}P chemical shifts (35.93 and 33.56 ppm for the PO_3/Mo_5 and PO_3/Mo_7 moieties, respectively). A third structure type of ODP/POM hybrid with ringlike or toroidal shape (Hybrid III, Figure 9C) can also be expected when two terminal PO_3 groups of a rodlike structure are bridged at both sides of a single Mo_5 cluster. Only a single ^{31}P resonance around 36 ppm is expected for these cyclic ODP/POM hybrids, because of their high symmetry. The discrimination between these various hybrids formed at higher $(NH_4)_6Mo_7O_{24}$ concentrations is not possible on the basis of their standard ^{31}P NMR spectra only but could be achieved by ^{31}P DOSY NMR.

^{31}P DOSY NMR

The DOSY data show that the diffusion coefficients associated with all signals gradually increase on increasing the $(NH_4)_6Mo_7O_{24}$ concentration above 14 mM (Figure 7, Table 2), and this implies that the newly formed ODP/POM hybrids are smaller and/or have different shapes. Our interpretation of this new trend in the diffusion coefficients at and above a $(NH_4)_6Mo_7O_{24}$:ODP ratio of 1:1 is that a formation of ODP/POM hybrids with shorter chains becomes increasingly favored again with further increases in $(NH_4)_6Mo_7O_{24}$ concentration.

To find the most probable averaged ODP/POM hybrids at each excess concentration of $(NH_4)_6Mo_7O_{24}$, we calculated the diffusion coefficients of rodlike Hybrids Ia, Ib, IIa, IIb, and IIc (Figure 9A and B) using Equation (6) and the optimized geometrical parameters a and b determined by MM calculations. Since no X-ray coordinates are available for phosphonate-bound Mo_7 clusters, we approximated the hybrid Mo_7 cluster ends with Mo_5 clusters. This should not affect significantly the values of the calculated diffusion coefficients, as the size differences between Mo_5 and Mo_7 clusters should be negligible with respect to the global size of the ODP/POM hybrids. The D_{calcd} values for hybrids with different numbers of ODP, Mo_5 clusters, and Mo_7 clusters, as well as the $(NH_4)_6Mo_7O_{24}$ concentrations at which the D_{calcd} values best match the D_{exptl} values, are given in Table 3. For reasons explained above for samples with an excess of ligand, we use only the D_{exptl} values determined from the most intense ^{31}P signal at 35.95 ppm. The results showed that the differences in D_{calcd} values for a given ODP/POM chain length terminated by 0, 1, or 2 Mo_7 units are insignificant, which makes their discrimination on the basis of their diffusion coefficients impossible. For example the D_{exptl} value of $0.87\times10^{-10}\,m^2\,s^{-1}$ measured for the composition with 14 mM $(NH_4)_6Mo_7O_{24}$ matches very well the D_{calcd} value for 8 ODP/7 Mo_5 hybrids terminated by 0, 1, or 2 Mo_7 clusters. However, the appearance of the signal at 33.56 ppm proves the presence of Mo_7-terminated hybrid chains, although only in very small amount at this sample composition, as evidenced by the very low intensity of the signal.

The overall analysis of the ^{31}P DOSY spectrum of the sample with 14 mM $(NH_4)_6Mo_7O_{24}$ reveals that it is a complex mixture in which the most represented ODP/POM hybrid best matching the experimental and calculated diffusion coefficients is Hybrid IIc with 8 ODP/7 Mo_5 units. A small amount of 8 ODP/7 POM hybrids terminated at one or both ends by an Mo_7 cluster (Hybrids IIb and IIa, respectively) is also present in the mixture.

The most probable ODP/POM hybrids were determined by using this approach for all sample compositions with excess POM. The results, summarized in Table 3, demonstrate that higher POM concentrations favor the formation of shorter-chain structures, most probably to compensate for the excess of POM. The formation of shorter hybrids effectively increases the relative amount of the thermodynamically more stable bound state of Mo_7 and Mo_5 clusters when the POM concentration greatly exceeds that of ODP.

Table 3. D_{calcd} values for hybrid structures with different numbers of ODP, Mo_5, and Mo_7 units and $(NH_4)_6Mo_7O_{24}$ concentration at which D_{calcd} best matches the D_{exptl} values for systems with excess $(NH_4)_6Mo_7O_{24}$ concentration. Diffusion coefficients given in bold are those that optimally match experimentally determined values. In the first three rows, no values for hybrids with 0 and 1 Mo_7 units are given, because unbound phosphonate moieties are not observed in the spectra of the samples with 60, 80, and 100 mM $(NH_4)_6Mo_7O_{24}$.

ODP units	Mo_5 units	Mo_7 units	$10^{10} D_{calcd}$ [$m^2 s^{-1}$]	$10^{10} D_{exptl}$ [$m^2 s^{-1}$]	$c(Mo_7)$ [mM]
1	0	2	2.90	2.76	100
2	1	2	**2.02**	2.08	100
				1.93	80
3	2	2	**1.62**	**1.71**	60
		0	1.36		
4	3	1	**1.32**	1.30	40
		2	**1.28**		
		0	1.18		
5	4	1	**1.15**	1.17	30
		2	1.12		
		0	1.05		
6	5	1	**1.03**	0.95	20
		2	**1.01**		
		0	**0.95**		
7	6	1	**0.93**	0.95	20
		2	**0.91**		
		0	**0.88**		
8	7	1	**0.86**	0.87	14
		2	0.85		
		0	0.81		
9	8	1	0.80	0.87	14
		2	0.79		
		0	0.76		
10	9	1	0.75	–	–
		2	0.74		
		0	0.71		
11	10	1	0.70	–	–
		2	0.69		

^{95}Mo NMR spectra

The formation of P_2Mo_5 units is supported by the appearance of a sharp ^{95}Mo resonance at −1.42 ppm in the ^{95}Mo spectrum of the mixture with 5.0 mM of $(NH_4)_6Mo_7O_{24}$ and 20 mM of ODP (Figure 10), showing that $[Mo_7O_{24}]^{6-}$ is mostly converted to P_2Mo_5 clusters. When the amount of $(NH_4)_6Mo_7O_{24}$ is further increased to 14 mM, P_2Mo_5 clusters still remain the dominant species. At this threshold concentration the reappearance of Mo_7 species is evidenced by the low-intensity ^{95}Mo signal around 33 ppm. However, the discrimination between bound and unbound Mo_7 clusters is not possible because of the small difference in their ^{95}Mo chemical shifts. Nevertheless, the ^{95}Mo signal around 33 ppm, together with the appearance of the ^{31}P resonance at 33.56 ppm, strongly supports the presence of bound Mo_7 clusters. The remaining two signals associated with unbound $[Mo_7O_{24}]^{6-}$ at 213 and 14 ppm are not observed because of the negligible amount of $[Mo_7O_{24}]^{6-}$ that is not converted to P_2Mo_5 clusters after reaction with ODP.

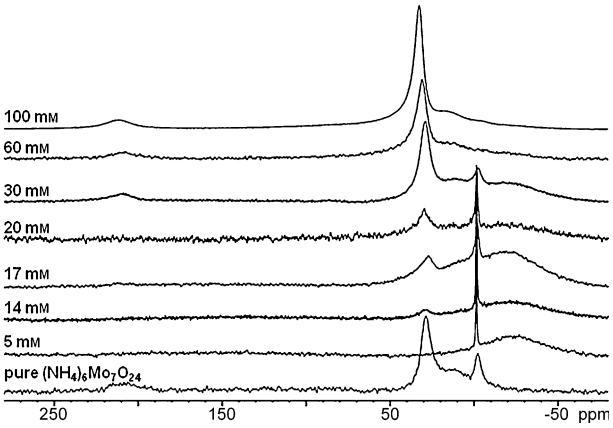

Figure 10. ^{95}Mo NMR spectra of pure POM (bottom line) and mixtures of 20 mM ODP and different amounts of $(NH_4)_6Mo_7O_{24}$.

In the presence of 17 and 20 mM of $(NH_4)_6Mo_7O_{24}$ the ^{95}Mo spectra show signals characteristic for both Mo_7 and Mo_5 clusters (Figure 10). At these concentrations only the most intense signal for Mo_7 species around 33 ppm is visible, while at higher $(NH_4)_6Mo_7O_{24}$ concentrations the other two, lower-intensity signals around 213 and 14 ppm are observable again. Unfortunately, due to the rather similar chemical shifts and the strong quadrupolar line broadening of the ^{95}Mo resonance, differentiation between the free and bound Mo_7 species is not possible. At the highest $(NH_4)_6Mo_7O_{24}$ concentrations used, the three signals of the unbound $[Mo_7O_{24}]^{6-}$ dominate the spectrum due to its large excess and hide the less intense peaks of the bound Mo_7 and Mo_5 clusters, as well as the broad hump for all other unbound Mo species. Nevertheless, the ^{31}P spectra unambiguously indicate the presence of bound Mo_7 and Mo_5 clusters at all $(NH_4)_6Mo_7O_{24}$ concentrations above 14 mM.

Toroidal structures

Increases in the experimental diffusion coefficients with increasing $(NH_4)_6Mo_7O_{24}$ concentration above 14 mM can a priori also be explained by the formation of toroidal ODP/POM hybrids (Hybrid III, Figure 9C). A simple model for the translational diffusion coefficient of a torus is given by Equation (7)[70]

$$D_t = \frac{k_B T}{\xi} = \frac{k_B T}{8\pi^2 \eta a}\left[\lg\left(\frac{8a}{b}\right) + \frac{1}{2}\right] \quad (7)$$

where η is the solvent viscosity, ξ the friction coefficient, a and b the geometrical parameters of the torus with slenderness ratio $\in = b/a$ (see Figure S6 of the Supporting Information for the definition of the torus geometrical parameters). Equation (7) is valid only under the assumption that translational and rotational degrees of freedom are decoupled and that

out-of-plane diffusion is much smaller than translational and twirling modes.

According to our MM calculations, a stable ring-shaped ODP/POM hybrid requires at least nine POM and nine ODP units. Table S2 (Supporting Information) summarizes the D_{calcd} values for toroidal ODP/POM hybrids with 9, 10, and 11 clusters, obtained by using Equation (7) and the MM geometrical parameters. The results demonstrate that these D_{calcd} values do not match the measured values at any sample composition. Consequently, toroidal hybrids can be ruled out on the basis of their much lower calculated diffusion coefficients in comparison to the experimental values.

Conclusion

We have demonstrated that polyoxometalate nanohybrids with controllable size and well-defined structure can be generated in excusively aqueous solution by tuning the pH and molar ratio of the polyoxometalate $(NH_4)_6Mo_7O_{24}$ and the organic ligand ODP. Multinuclear (^{1}H, ^{31}P, and ^{95}Mo) NMR analysis in combination with ^{31}P DOSY experiments and molecular mechanics calculations, enabled detailed characterization of the structure, size, and shape of the hybrids obtained at different sample compositions. The bifunctionality of the organic ligand allowed formation of rodlike oligomeric structures with variable numbers of covalently bound ODP/POM units, depending on the molar ratio of the organic ligand and POM. The results show that, in the presence of an excess of the bifunctional organic ligand, the ODP/POM hybrid chains are terminated by unbound phosphonate moieties at both ends. The terminal unbound phosphonate groups enable further interaction of the hybrid chains with Mo_5 clusters, and their length increases on further increasing the POM concentration. With an excess of $(NH_4)_6Mo_7O_{24}$, the formation of shorter chains terminated at one or both ends by Mo_7 clusters is favored, and the length of the ODP/POM hybrids decreases with increasing $(NH_4)_6Mo_7O_{24}$ concentration. This strategy, based on integrating ^{31}P DOSY NMR and MM calculations, was used as a novel tool to determine nanohybrid size and shape. This approach is a powerful tool in the field of polyoxometalate chemistry, in which up to now it has been virtually unexploited. Here we have demonstrated its usefulness and applicability for detailed structural characterization of functionalized organic–inorganic POM-based hybrids in solution.

Experimental Section

Sample preparation

1,8-Octanediphosphonic acid (ODP), ammonium heptamolybdate ($(NH_4)_6Mo_7O_{24}$), and sodium molybdate (Na_2MoO_4) were purchased form Sigma-Aldrich, Acros Organics, and Chem-Lab, respectively. All products were used without further purification.

ODP solutions (20 mM) were prepared by dissolving ODP (5.5 mg) in D_2O (1.0 mL). The desired amount of ammonium heptamolybdate (2–100 mM) was added as a solid to this solution and the pD value was adjusted to 5.0 by adding small amounts of concentrated DCl (20 wt%) and NaOD (40 wt%). The pH-meter reading was corrected by using the equation pD = pH + 0.41.[71]

Standard and DOSY NMR data acquisition and processing

The ^{1}H, ^{31}P, and DOSY NMR measurements were performed on a Bruker Avance II+ 600 NMR spectrometer, equipped with 5 mm dual ^{1}H/^{31}P Diff30 probe and a 40A gradient amplifier, providing a maximum gradient strength of 11.8 T m^{-1}. ^{1}H NMR spectra were acquired with 32*k* time domain points, a spectral width of 7200 Hz, and 128 scans. The ^{31}P spectra were recorded with 64*k* time-domain data points, a spectral width of 50 kHz, a relaxation delay of 15 s, 128 scans, and referenced to external 85% H_3PO_4 in a capillary. The inverse-gated decoupling ensured quantitative signal-area measurements. The ^{31}P DOSY spectra were acquired with the Diff suite integrated in the Topspin package by using the double-stimulated echo pulse sequence[72] to compensate for possible convection during the experiments. The inverse-gated decoupling scheme was implemented in the standard convection-compensated DOSY pulse sequence to increase the sensitivity by eliminating $^{2/3}J(^1H–^{31}P)$ scalar couplings. Monopolar sine-shaped gradient pulses, a gradient recovery delay τ of 100 μs, a longitudinal eddy current delay of 20 ms, and three spoiling gradients were utilized. A diffusion delay Δ of 100 ms and a gradient pulse length δ of 1 ms were used. The gradient strength *G* was varied in 32 linear steps from 35.4 to 283.6 G cm^{-1} to ensure complete signal attenuation. All spectra were recorded without sample spinning with 16*k* time-domain data points in the t_2 dimension, 128 transients for each gradient increment, and a relaxation delay of 5 s. To minimize the effects of external temperature variations, the air conditioning in the laboratory and the air flow to the probe were switched off. The water-cooling system of the Diff30 probe, set to 25 °C, was used to regulate the sample temperature. Experiments were started one hour after insertion of the sample into the magnet to minimize temperature drift. The spectra were processed with an exponential window function (line broadening factor 1), 64*k* data points in the F2 dimension, and 1*k* data points in the diffusion dimension, by using the fitting routine integrated in TopSpin3.1 package. The diffusion coefficients were calculated by fitting the sum of the columns along the chemical shift of each signal in the DOSY spectrum with the Gaussian distribution curve. The ^{95}Mo NMR spectra were recorded on a Bruker Avance II+ 600 NMR spectrometer equipped with a 10 mm PA BBO 600-B BBLR-H-D-10 Z probe with 32*k* time-domain points, a spectral width of 156.250 kHz, and Na_2MoO_4 (2 M) as external reference.

Molecular mechanics calculations

Molecular mechanics calculations on model ODP/POM hybrids containing 1–10 $[P_2Mo_5O_{21}]^{4-}$ cluster units were performed for the purpose of modeling the hybrids as cylinders amenable to estimations of calculated diffusion coefficients for comparison with the diffusion coefficients determined experimentally by DOSY NMR. Although DFT calculations proved to be suitable for describing structural and physical properties of POMs,[73,74] the size of the systems under investigation, with up to ten clusters, makes the application of quantum mechanical methods too computationally demanding. Therefore, MM methods were preferred. Another reason for adopting MM is that no detailed electronic structure is required for the purpose of obtaining only molecular sizes and shapes of the hybrids to calculate their diffusion coefficients. Among the many force fields currently available in inorganic chemistry,[75] the universal force field (UFF)[63] was selected because it provided reliable results for many inorganic systems.[76;77] Moreover, it includes full pa-

rameterization for all elements in the Mo POM clusters of interest, which enabled us to investigate straightforwardly all ODP/POM nanohybrids of interest within affordable computational times. The UFF version implemented in the Gaussian 09 computational package was used.[78] The initial cluster geometries were taken from X-ray data available in the literature.[64]

Acknowledgements

R.W. and T.P.-V. are indebted to the Fund of Scientific Research Flanders (FWO, Belgium, grant G.0029.10N) for financial support. R.W. and P.S. acknowledge financial support from the bilateral cooperation agreement between the Bulgarian Academy of Sciences (BAS) and the FWO (grant VS.016.10N). R.W. acknowledges financial support from the Research Council of the Vrije Universiteit Brussel (OZR-VUB; Grant GOA31), having made possible several stays of P.S. at the VUB. G.A. acknowledges the FWO for the postdoctoral fellowship. P.S. acknowledges the financial support of National Science Fund, Ministry of Education and Science of Bulgaria, infrastructure project DRNF 02/13/2009 "Bulgarian NMR Centre – Development of Advanced and Effective Research Infrastructure for NMR Analysis of Bio- and Nanomaterials". F.D.P. wishes to acknowledge the Research Foundation Flanders (FWO) and the Vrije Universiteit Brussel (VUB) for continuous support to his group. F.D.P. and F.M.M. also acknowledge financial support from the Research Council of the Vrije Universiteit Brussel (OZR-VUB; Grant GOA77 grant and a Strategic Research Program). All authors are indebted to M. Petitjean, Université D. Diderot, Paris 6, for his kind assistance in the application of his algorithm to the needs of this work, in particular by making available his software. The authors acknowledge the CMST COST Action CM1203 (Polyoxometalate Chemistry for Molecular Nanoscience) for the financial support in terms of STMS applications. The authors also wish to acknowledge Stoyan Denkov for his time and effort in making the back cover illustration artwork.

Keywords: diffusion NMR spectroscopy · molecular mechanics · nanohybrids · polyoxometalates · shape factor

[1] D. L. Long, R. Tsunashima, L. Cronin, *Angew. Chem.* **2010**, *122*, 1780 – 1803; *Angew. Chem. Int. Ed.* **2010**, *49*, 1736 – 1758.
[2] A. Proust, R. Thouvenot, P. Gouzerh, *Chem. Commun.* **2008**, 1837 – 1852.
[3] I. Kozhevnikov, *Catalysis by polyoxometalates*; John Wiley & Sons, Chichester, **2002**, Vol. 2.
[4] B. Hasenknopf, *Front. Biosci.* **2005**, *10*, 275 – 287.
[5] H. Yanagie, A. Ogata, S. Mitsui, T. Hisa, T. Yamase, M. Eriguchi, *Biomed. Pharmacother.* **2006**, *60*, 349 – 352.
[6] H. Stephan, M. Kubeil, F. Emmerling, C. E. Müller, *Eur. J. Inorg. Chem.* **2013**, 1585 – 1594.
[7] Y. F. Song„ R. Tsunashima, *Chem. Soc. Rev.* **2012**, *41*, 7384 – 7402.
[8] H. N. Miras, J. Yan, D.-L. Long, L. Cronin, *Chem. Soc. Rev.* **2012**, *41*, 7403 – 7430.
[9] Y.-F. Song, N. McMillan, D.-L. Long, J. Thiel, Y. Ding, H Chen, .N. Gadegaard, L. Cronin, *Chem. Eur. J.* **2008**, *14*, 2349 – 2354.
[10] J. Zhang, Y. F. Song, L. Cronin, T. B. Liu, *J. Am. Chem. Soc.* **2008**, *130*, 14408 – 14409.
[11] J. Zhang, Y. F. Song, L. Cronin, T. B. Liu, *Chem. Eur. J.* **2010**, *16*, 11320 – 11324.
[12] P. Yin, C. P. Pradeep, B. Zhang, F.-Y. Li, C. Lydon, M. H. Rosnes, D. Li, E. Bitterlich, L. Xu, L. Cronin, T. Liu, *Chem. Eur. J.* **2012**, *18*, 8157 – 8162.
[13] Y. K. Han, Y. Xiao, Z. J. Zhang, B. Liu, P Zheng, S. J. He, W. Wang, *Macromolecules* **2009**, *42*, 6543 – 6548.
[14] C. P. Pradeep, M. F. Misdrahi, F. Y. Li, J. Zhang, L. Xu, D. L. Long, T. B. Liu, L. Cronin, *Angew. Chem.* **2009**, *121*, 8459 – 8463; *Angew. Chem. Int. Ed.* **2009**, *48*, 8309 – 8313.
[15] C. P. Pradeep, F.-Y. Li, C. Lydon, H. N. Miras, D.-L. Long, L. Xu, L. Cronin, *Chem. Eur. J.* **2011**, *17*, 7472 – 7479.
[16] P. C. Yin, P. F. Wu, Z. C. Xiao, D. Li, E. Bitterlich, J. Zhang, P. Cheng, D. V. Vezenov, T. B. Liu, Y. G. Wei, *Angew. Chem.* **2011**, *123*, 2569 – 2573; *Angew. Chem. Int. Ed.* **2011**, *50*, 2521 – 2525.
[17] M. F. Misdrahi, M. Wang, C. P. Pradeep, F.-Y. Li, C. Lydon, L. Xu, L. Cronin, T. Liu, *Langmuir* **2011**, *27*, 9193 – 9202.
[18] S. Landsmann, C. Lizandara-Pueyo, S. Polarz, *J. Am. Chem. Soc.* **2010**, *132*, 5315 – 5321.
[19] L. Pettersson, I. Andersson, L. O. Ohman, *Inorg. Chem.* **1986**, *25*, 4726 – 4733.
[20] L. Pettersson, *Acta Chem. Scand.* **1971**, *25*, 1959 – 1974.
[21] R. Strandberg, *Acta Chem. Scand.* **1973**, *27*, 1004 – 1018.
[22] E. Cartuyvels, G. Absillis, T. N. Parac-Vogt, *Chem. Commun.* **2008**, 85 – 87.
[23] L. Van Lokeren, E. Cartuyvels, G. Absillis, R. Willem, T. N. Parac-Vogt, *Chem. Commun.* **2008**, 2774 – 2776.
[24] G. Absillis, R. Van Deun, T. N. Parac-Vogt, *Inorg. Chem.* **2011**, *50*, 11552 – 11560.
[25] G. Absillis, E. Cartuyvels, R. Van Deun, T. N. Parac-Vogt, *J. Am. Chem. Soc.* **2008**, *130*, 17400 – 17408.
[26] W. Kwak, M. T. Pope, T. F. Scully, *J. Am. Chem. Soc.* **1975**, *97*, 5735 – 5738.
[27] A. Kobayashi, A. Yagasaki, *Polyhedron* **1998**, *17*, 3315 – 3320.
[28] A. Yagasaki, I. Andersson, L. Pettersson, *Inorg. Chem.* **1987**, *26*, 3926 – 3933.
[29] U. Kortz, M. T. Pope, *Inorg. Chem.* **1995**, *34*, 2160 – 2163.
[30] M. Carraro, A. Sartorel, G. Scorrano, C. Maccato, M. H. Dickman, U Kortz, M. Bonchio, *Angew. Chem.* **2008**, *120*, 7385 – 7389; *Angew. Chem. Int. Ed.* **2008**, *47*, 7275 – 7279.
[31] R. D. Adams, W. G. Klemperer, R. S. Liu, *J. Chem. Soc. Chem. Commun.* **1979**, 256 – 257.
[32] P. R. Marcoux, B. Hasenknopf, J. Vaissermann, P. Gouzerh, *Eur. J. Inorg. Chem.* **2003**, 2406 – 2412.
[33] C. V. Di Anibal, M. A. Moroni, V. Verdinelli, J. Luis Rodriguez, R. Minardi, P. C. Schulz, B. Vuano, *Colloids Surf. A* **2009**, *348*, 276 – 281.
[34] K. F. Morris, C. S. Johnson, *J. Am. Chem. Soc.* **1992**, *114*, 3139 – 3141.
[35] K. F. Morris, C. S. Johnson, *J. Am. Chem. Soc.* **1993**, *115*, 4291 – 4299.
[36] C. S. Johnson, *Prog. Nucl. Magn. Reson. Spectrosc.* **1999**, *34*, 203 – 256.
[37] K. Ulrich, M. Sanders, F. Grinberg, P. Galvosas, S. Vasenkov, *Langmuir* **2008**, *24*, 7365 – 7370.
[38] M. Valentini, A. Vaccaro, A. Rehor, A. Napoli, J. A. Hubbell, N. Tirelli, *J. Am. Chem. Soc.* **2004**, *126*, 2142 – 2147.
[39] T. J. Zhao, H. W. Beckham, *Macromolecules* **2003**, *36*, 9859 – 9865.
[40] P. S. Denkova, L. Van Lokeren, R. Willem, *J. Phys. Chem. B* **2009**, *113*, 6703 – 6709.
[41] P. Denkova, D. Momekova, S. Rangelov, N. Lambov, R. Willem, *J. Controlled Release* **2010**, *148*, E47 – E48.
[42] A. Kowalczuk, E. Stoyanova, V. Mitova, P. Shestakova, G. Momekov, D. Momekova, N. Koseva, *Int. J. Pharm.* **2011**, *404*, 220 – 230.
[43] Y. Cohen, L. Avram, L. Frish, *Angew. Chem.* **2005**, *117*, 524 – 560; *Angew. Chem. Int. Ed.* **2005**, *44*, 520 – 554.
[44] A. Pastor, E. Martinez-Viviente, *Coord. Chem. Rev.* **2008**, *252*, 2314 – 2345.
[45] S. Han, Z. Ma, R. Hopson, Y. Wei, D. Budil, S. Gulla, B. Moulton, *Inorg. Chem. Commun.* **2012**, *15*, 78 – 83.
[46] I. Fernández, E. Martinez-Viviente, F. Breher, P. S. Pregosin, *Chem. Eur. J.* **2005**, *11*, 1495 – 1506.
[47] E. Martinez-Viviente, H. Ruegger, P. S. Pregosin, J. Lopez-Serrano, *Organometallics* **2002**, *21*, 5841 – 5846.
[48] D. Nama, P. G. A. Kumar, P. S. Pregosin, *Magn. Reson. Chem.* **2005**, *43*, 246 – 250.
[49] J.-F. Lemonnier, S. Floquet, A. Kachmar, M.-M. Rohmer, M. Benard, J. Marrot, E. Terazzi, C. Piguet, E. Cadot, *Dalton Trans.* **2007**, 3043 – 3054.
[50] S. Floquet, S. Brun, J.-F. Lemonnier, M. Henry, M.-A. Delsuc, Y. Prigent, E. Cadot, F. Taulelle, *J. Am. Chem. Soc.* **2009**, *131*, 17254 – 17259.

[51] J.-F. Lemonnier, S. Floquet, J. Marrot, E. Terazzi, C. Piguet, P. Lesot, A. Pinto, E. Cadot, *Chem. Eur. J.* **2007**, *13*, 3548 – 3557.
[52] M. V. Vasylyev, S. Gatard, I. Bar-Nahum, L. Konstantinovski, E. J. Wachtel, R. Neumann, *J. Cluster Sci.* **2006**, *17*, 235 – 243.
[53] M.-P. Santoni, A. K. Pal, G. S. Hanan, M.-C. Tang, K. Venne, A. Furtos, P. Menard-Tremblay, C. Malveau, B. Hasenknopf, *Chem. Commun.* **2012**, *48*, 200 – 202.
[54] D. G . Lyxell, L. Pettersson, I. Persson, *Inorg. Chem.* **2001**, *40*, 584 – 592.
[55] R. I. Maksimovskaya, G. M. Maksimov, *Inorg. Chem.* **2007**, *46*, 3688 – 3695.
[56] A. Einstein, *Ann. Phys.* **1905**, *322*, 549 – 560.
[57] H. Brenner, *Int. J. Multiphas. Flow* **1974**, *1*, 195 – 341.
[58] P. C. Hiemenz, *Principles of Colloid and Surface Chemistry*, Marcel Dekker, New York, **1986**.
[59] V. Bloomfield, *On-line Biophysics Textbook*; Vol. Separation and Hydrodynamics, **2000**.
[60] J. G. de la Torre, V. A. Bloomfield, *Q. Rev. Biophys.* **1981**, *14*, 81 – 139.
[61] M. M. Tirado, C. L. Martinez, J. G. de La Torre, *J. Chem. Phys.* **1984**, *81*, 2047 – 2052.
[62] A. Ortega, J. G. de La Torre, *J. Chem. Phys.* **2003**, *119*, 9914 – 9919.
[63] A. K. Rappe, C. J. Casewit, K. S. Colwell, W. A. Goddard, W. M. Skiff, *J. Am. Chem. Soc.* **1992**, *114*, 10024 – 10035.
[64] D.-G. Lyxell, R. Strandberg, *Acta Crystallogr. Sect. A Acta Crystallogr. Sect. C-Cryst. Struct. Commun.* **1988**, *44*, 1535 – 1538.
[65] M. Petitjean, *Appl. Algebr. Eng. Commun. Comput.* **2012**, *23*, 151 – 164.
[66] T. Riis-Johannessen, G. Bernardinelli, Y. Filinchuk, S. Clifford, N. D. Favera, C. Piguet, *Inorg. Chem.* **2009**, *48*, 5512 – 5525.
[67] S. Hou, S. A. Wieczorek, T. S. Kaminski, N. Ziebacz, M. Tabaka, N. A. Sorto, M. H. Foss, J. T. Shaw, M. Thanbichler, D. B. Weibel, K. Nieznanski, R. Holyst, P. Garstecki, *J. Biol. Chem.* **2012**, *287*, 23878 – 23886.
[68] A. Chen, D. H. Wu, C. S. Johnson, *J. Am. Chem. Soc.* **1995**, *117*, 7965 – 7970.
[69] J. Viéville, M. Tanty, M.-A. Delsuc, *J. Magn. Reson.* **2011**, *212*, 169 – 173.
[70] R. M. Thaokar, *Colloids Surf. A* **2008**, *317*, 650 – 657.
[71] A. K. Covington, M. Paabo, R. A. Robinson, R. G. Bates, *Anal. Chem.* **1968**, *40*, 700 – 706.
[72] A. Jerschow, N. Muller, *J. Magn. Reson.* **1997**, *125*, 372 – 375.
[73] A. J. Bridgeman, G. Cavigliasso, *Dalton Trans.* **2002**, 2244 – 2249.
[74] A. J. Bridgeman, G. Cavigliasso, *Inorg. Chem.* **2002**, *41*, 1761 – 1770.
[75] P. Comba, R. Remenyi, *Coord. Chem. Rev.* **2003**, *238 – 239*, 9 – 20.
[76] A. K. Rappe, K. S. Colwell, C. J. Casewit, *Inorg. Chem.* **1993**, *32*, 3438 – 3450.
[77] G. Garberoglio, S. Taioli, *Microporous Mesoporous Mater.* **2012**, *163*, 215 – 220.
[78] Gaussian 09, M. J. T. Frisch, G. W. Trucks, H. B. Schlegel, G. E. Scuseria, M. A. Robb, J. R. Cheeseman, G. Scalmani, V. Barone, B. Mennucci, G. A. Petersson, H. Nakatsuji, M. Caricato, X. Li, H. P. Hratchian, A. F. Izmaylov, J. Bloino, G. Zheng, J. L. Sonnenberg, M. Hada, M. Ehara, K. Toyota, R. Fukuda, J. Hasegawa, M. Ishida, T. Nakajima, Y. Honda, O. Kitao, H. Nakai, T. Vreven, J. A. Montgomery, Jr., J. E. Peralta, F. Ogliaro, M. Bearpark, J. J. Heyd, E. Brothers, K. N. Kudin, V. N. Staroverov, R. Kobayashi, J. Normand, K. Raghavachari, A. Rendell, J. C. Burant, S. S. Iyengar, J. Tomasi, M. Cossi, N. Rega, J. M. Millam, M. Klene, J. E. Knox, J. B. Cross, V. Bakken, C. Adamo, J. Jaramillo, R. Gomperts, R. E. Stratmann, O. Yazyev, A. J. Austin, R. Cammi, C. Pomelli, J. W. Ochterski, R. L. Martin, K. Morokuma, V. G. Zakrzewski, G. A. Voth, P. Salvador, J. J. Dannenberg, S. Dapprich, A. D. Daniels, Ö. Farkas, J. B. Foresman, J. V. Ortiz, J. Cioslowski, D. J. Fox, Revision A.1 ed.; Gaussian, Inc.: Wallingford CT, **2009**.

Received: December 19, 2013
Published online on ■■ ■■, 0000

FULL PAPER

Organic–Inorganic Hybrids

*P. Shestakova, G. Absillis, F. J. Martin-Martinez, F. De Proft, R. Willem, T. N. Parac-Vogt**

■■ – ■■

Integrating ^{31}P DOSY NMR Spectroscopy and Molecular Mechanics as a Powerful Tool for Unraveling the Chemical Structures of Polyoxomolybdate-Based Amphiphilic Nanohybrids in Aqueous Solution

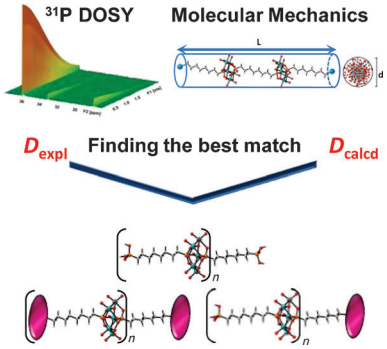

Rodlike organic–inorganic hybrids with variable numbers of covalently bound 1,8-octanediphosphonic acid (ODP) and polyoxomolybdate $(NH_4)_6Mo_7O_{24}$ (POM) units were generated in aqueous solution. The structure, size, and shape of the ODP/POM hybrids as a function of ODP:POM molar ratio were determined by ^{31}P DOSY NMR and molecular mechanics calculations, in combination with ^{1}H, ^{31}P, and ^{95}Mo NMR spectroscopy. Comparison of the calculated (D_{calcd}) and experimentally determined diffusion coefficients (D_{exptl}) led to the most probable ODP/POM hybrid length for each sample composition (see figure).

It looks like magic.....but in the end it's all straightforward! Linear polyoxometalate based hybrids have been synthesized by simply mixing $(NH_4)_6Mo_7O_{24}$ and 1,8-octanediphosphonic acid in aqueous solution. By using a multi-technique approach, combining ^{31}P DOSY, ^{95}Mo NMR spectroscopy and molecular mechanics calculations, the nature and length of these hybrids were determined. For more details, see the Full Paper by T. N. Parac-Vogt et al. on p. ■■■■ ff.